Reduced-order Modeling and Dynamic Stability Analysis of MTDC Systems in DC Voltage Control Timescale

Li Guo, *Member, IEEE*, Pengfei Li, Xialin Li, *Member, IEEE*, Fei Gao, *Member, IEEE*, Di Huang, and Chengshan Wang, *Senior Member, IEEE*

***Abstract*—An equivalent source-load MTDC system including DC voltage control units, power control units and interconnected DC lines is considered in this paper, which can be regarded as a generic structure of low-voltage DC microgrids, medium-voltage DC distribution systems or HVDC transmission systems with a common DC bus. A reduced-order model is proposed with a circuit structure of a resistor, inductor and capacitor in parallel for dynamic stability analysis of the system in DC voltage control timescale. The relationship between control parameters and physical parameters of the equivalent circuit can be found, which provides an intuitive insight into the physical meaning of control parameters. Employing this model, a second-order characteristic equation is further derived to investigate system dynamic stability mechanisms in an analytical approach. As a result, the system oscillation frequency and damping are characterized in a straight forward manner, and the role of electrical and control parameters and different system-level control strategies in system dynamic stability in DC voltage control timescale is defined. The effectiveness of the proposed reduced-order model and the correctness of the theoretical analysis are verified by simulation based on PSCAD/EMTDC and an experiment based on a hardware low-voltage MTDC system platform.**

***Index Terms*—DC voltage control timescale, dynamic stability, equivalent source-load MTDC system, reduced-order model, second-order characteristic equation.**

I. Introduction

WITH integration of a large-scale renewable distributed generators (DGs) and DC sources and loads, a flexible DC interconnection based multi-terminal (MTDC) system as an effective implementation form of a low-voltage DC microgrid (MG), medium-voltage DC distribution system and HVDC transmission system, has developed rapidly in the past decade [1]–[3]. It can integrate with distributed resources, energy storage devices and loads effectively, and realize flexible interlinking of AC and DC systems, and multi-area coordinated control by interlinking converters (ICs) [4], [5].

MTDC systems can operate in master-slave control [6], [7] and droop control [8], [9]. While no matter which system-level control strategy is used, maintaining good system dynamic stability is the basic premise for the safety and reliability of system operation. Essentially, MTDC systems in practical application scenarios can be regarded as equivalent source-load MTDC systems including DC voltage control units, power control units and interconnected DC lines. DC voltage control units are used to control DC voltage stability and maintain power balance as "Source". "Load" refers to generic constant power load (CPL) units, which can be DGs or power electronics-based interfaces under power control and DC loads, and the direction of power flow can be positive or negative. Due to complex structure, interaction dynamic of multi-controllers and multi-timescale coupling, how to model the equivalent source-load MTDC system reasonably and effectively, and further analyze system dynamic stability are the main motivations of this paper.

From the perspective of system stability, a lot of research has been carried out on high-frequency oscillation issues, which are usually caused by dynamic interaction between the negative-resistance characteristic of CPLs and *LC* filters. And resonance mechanism analysis and damping control have been studied in [10]–[12]. However, in this paper, we focus on the system dynamic stability mechanism in DC voltage control (DVC) timescale, which ignores the influence of inner current control with fast dynamic. "DVC timescale" is first proposed by Yuan and his team and a lot of fruitful studies have been done [13]–[17]. Based on motion equation concept, the stability of a grid-connected system in weak grid condition was analyzed in [13]. Reference [14] provided a physical insight into VSC stability issues by introducing the concept of "damping power and synchronizing power." These studies focus on the stability mechanism of grid-connected VSC systems, especially in weak condition, rather than the dynamic stability of DC systems. Moreover, some issues still need to be solved, such as why it is called "DC voltage control timescale," and what are the key factors of system dynamic stability in DVC timescale.

From the viewpoint of methodology, "impedance-based" "state-space" and "close-loop transfer function" are traditional methods which can be used to stability analysis in DVC

Manuscript received September 29, 2019; revised December 22, 2019; accepted January 7, 2020. Date of online publication February 13, 2020; date of current version April 27, 2020. This work was supported in part by the National Natural Science Foundation of China under Grant No. 51977142.

L. Guo, P. F. Li, X. L. Li (corresponding author, e-mail: xialinlee@tju.edu.cn), and C. S. Wang are with the Key Laboratory of Smart Grid of Ministry of Education, Tianjin University, Tianjin 300072, China.

F. Gao is with Shanghai Jiao Tong University, Shanghai 200240, China.

D. Huang is with Guangzhou Power Supply Bureau of Guangdong Power Grid Co., Ltd., Guangzhou 510620, China.

DOI: 10.17775/CSEEJPES.2019.02350

timescale. Nyquist criterion, Middle brook criterion and their improved criterions can be used for "impedance-based" stability analysis [18]–[20]. In [20], a complete system impedance matrix was derived to investigate high-frequency oscillation in DC MGs considering multiple types of DGs and loads. However, the aforementioned modeling method can only provide stability information with numerical results, which cannot be adopted for system dynamic stability analysis in an analytical approach.

By linearizing the detailed system model, the "state-space" model can be derived, then eigenvalues, parameter sensitivity analysis, and then the participation factor can be used to analyze system stability [21]–[23]. In [23], a linearized model was used for the stability analysis of a low-voltage DC MG considering multi-source and multi-load. To reduce model order, the proposed model only considered the influence of droop control. An alternative method for stability analysis is to obtain close-loop transfer functions and further calculate the roots [24]–[26]. In [25], the close-loop transfer function of a cluster with multiple MGs was established, and the influence of control parameters on system stability was analyzed through root locus. However, the state-space model and close-loop transfer functions are both inherently numeral calculation based methods due to high-order modeling. They are difficult to provide an intuitive insight into the dynamic stability of MTDC systems in DVC timescale.

In other words, the above mentioned methods can only provide stability information with numerical results, which cannot uncover the system dynamic stability in an analytical approach. Therefore, the main innovations of the paper can be summarized as:

1) An equivalent parallel *RLC* model is derived for dynamic stability of the MTDC system in DVC timescale. The DC voltage control unit is modeled as an equivalent current source with a circuit of a resistor, inductor and capacitor in parallel by ignoring the droop control. It is easy to find the relationship between control parameters and physical parameters of the equivalent circuit, and the physical meaning of control parameters can be revealed intuitively.

2) Impedance ratios $K(s)$ and $L(s)$ are introduced to modify the equivalent model considering droop control and DC lines based on their amplitude-frequency characteristics. $K(s)$ is simplified to a first-order high-pass filter for a DC voltage control unit, and $L(s)$ equaling 1 is adopted for a generic CPL unit, which not only reduces the model order, but also retains the model accuracy for dynamic stability.

3) Based on the modified model of the system, the second-order characteristic equation has been further obtained, which makes it easy to study system damping and oscillation frequency intuitively. And the role of electrical and control parameters in system dynamic stability is defined.

4) The system dynamic stability with different system-level control strategies (master-slave control and droop based peer-to-peer control) is investigated.

This paper is organized as follows. Section II presents the topology and control of the system. The proposed reduced-order modeling method is provided in Section III. Model verification and analysis are given in Section IV. A low-voltage MTDC system platform based experimental verification is carried out in Section V. Section VI concludes the paper.

II. Topology and Control of MTDC Systems

The MTDC system considered in this paper is shown in Fig. 1 [27]. DC voltage control units are used to control DC voltage stability and maintain power balance as "Source". "Load" refers to generic constant power load (CPL) units. $u_{\rm com}$ is the voltage of the common DC bus. In addition, DC voltage control units and generic CPL units are interconnected with the common DC bus through the corresponding DC lines. Master-slave control and droop based peer-to-peer control can be used in this system, and the number of DC voltage control units differs in the two modes.

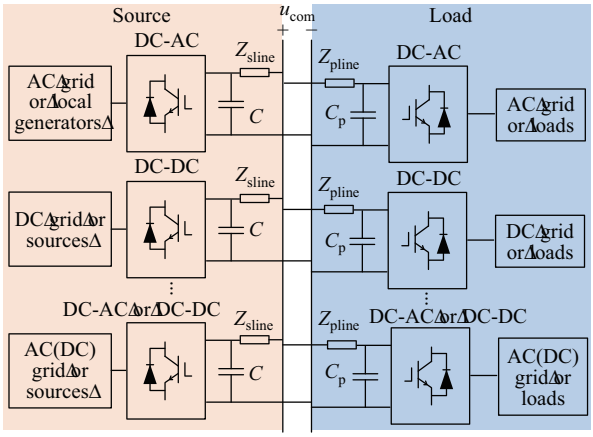

Fig. 1. Topology of the MTDC system.

The control system of the DC voltage control unit #i ($i = 1, 2, \ldots, n$) is composed of droop control, DC voltage control and inner current control shown in Fig. 2. $R_{{\rm sline}i}$ and $L_{{\rm sline}i}$ are DC line resistance and inductance respectively; C_{si} is DC capacitance at the side of the common DC bus; $u_{{\rm dcset}i}$ and $u_{{\rm dc}i}$ are the reference and actual value of the DC voltage; $i_{{\rm dcset}i}$ and $i_{{\rm odc}i}$ are DC current setting value and actual value; and i_{si} is the AC current of the DC voltage control unit. Droop controller $G_{\rm d}(s)$ is designed as:

$$G_{\rm d}(s) = R_{\rm d}/(1 + T_{\rm lpf}s) \tag{1}$$

where $R_{\rm d}$ and $T_{\rm lpf}$ are droop gain and low-pass filter constant.

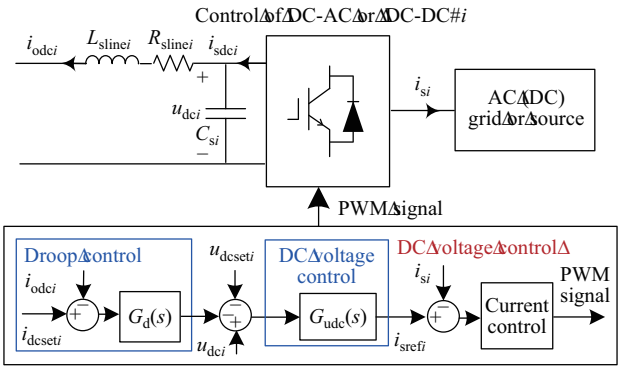

Fig. 2. Control of the DC voltage control unit.

PI control is adopted in the DC voltage controller $G_{\rm udc}(s)$, which can be described as:

$$G_{\rm udc}(s) = k_{\rm pu} + k_{\rm iu}/s \tag{2}$$

where $k_{\rm pu}$ and $k_{\rm iu}$ are proportional gain and integral gain.

III. Reduced-order Modeling

This paper primarily investigates the dynamic stability of the MTDC system in DVC timescale, the inner current control can be ignored as its dynamic is almost 10 times faster than the DC voltage control dynamic [14]. Note that the reduced-order modeling method is based on per-unit (pu) system.

A. Modeling of DC Voltage Control Unit

Without considering inner current control with fast dynamic, the transfer function of the DC voltage control unit is shown in Fig. 3. DC voltage dynamic in a small signal manner is:

$$\begin{aligned}\Delta u_{{\rm dc}i} &= \frac{G_{\rm udc}(s)}{sC_{{\rm s}i}+G_{\rm udc}(s)}\Delta u_{{\rm dcset}i} - \frac{1}{sC_{{\rm s}i}+G_{\rm udc}(s)}\Delta i_{{\rm odc}i} \\ &\quad - \frac{G_{\rm udc}(s)G_{\rm d}(s)}{sC_{{\rm s}i}+G_{\rm udc}(s)}(\Delta i_{{\rm odc}i} - \Delta i_{{\rm dcset}i}) \\ &= \Delta U_{{\rm ref}i} - Z_{{\rm s}i}\Delta i_{{\rm odc}i} - Z_{{\rm sdroop}i}(\Delta i_{{\rm odc}i} - \Delta i_{{\rm dcset}i})\end{aligned} \tag{3}$$

where $\Delta U_{{\rm ref}i}$ represents the equivalent voltage source of the DC voltage control unit, $Z_{{\rm s}i}$ is the output impedance by ignoring droop control, and $Z_{{\rm sdroop}i}$ represents the impedance related to droop control.

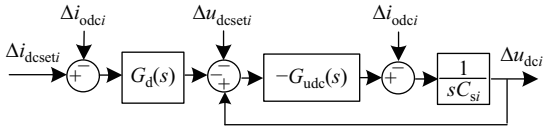

Fig. 3. Transfer function of the DC voltage control unit.

The equivalent circuit model of the DC voltage control unit based on the Norton theorem can be obtained from (3) shown in Fig. 4(a). And the impedance $Z_{{\rm s}i}$ can be described as:

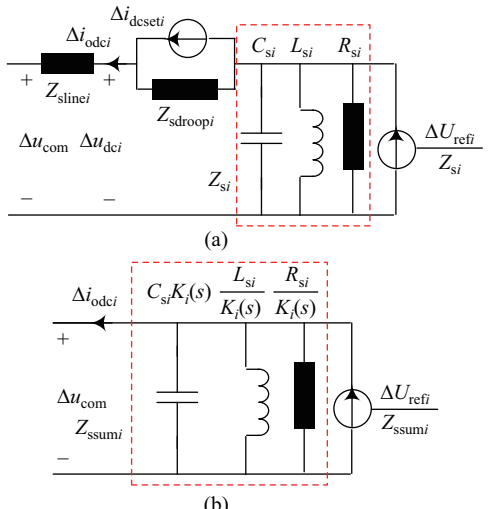

Fig. 4. Evolution of reduced-order model of the DC voltage control unit. (a) The basic model. (b) The model by introducing $K_i(s)$.

$$1/Z_{{\rm s}i} = 1/R_{{\rm s}i} + 1/(L_{{\rm s}i}s) + sC_{{\rm s}i} \tag{4}$$

where $R_{{\rm s}i} = 1/k_{\rm pu}$, $L_{{\rm s}i} = 1/k_{\rm iu}$.

From (4), the equivalent impedance $Z_{{\rm s}i}$ is inherently composed of a resistor, inductor and capacitor in parallel. It is easy to find the relationship between control parameters and physical parameters of the equivalent circuit, and the physical meaning of control parameters is revealed intuitively. Considering DC line impedance $Z_{{\rm sline}i}$ and $Z_{{\rm sdroop}i}$ related to droop control, in order to retain the parallel *RLC* structure, the model in Fig. 4(a) can be further modified as shown in Fig. 4(b), and the coefficient $K_i(s)$ is defined as:

$$K_i(s) = Z_{{\rm s}i}/(Z_{{\rm s}i} + Z_{{\rm sline}i} + Z_{{\rm sdroop}i}) = Z_{{\rm s}i}/Z_{{\rm ssum}i} \tag{5}$$

It is obvious that $K_i(s)$ is inherently an impedance ratio of the DC voltage control unit.

B. Modeling of Generic CPL Unit

In the considered system, the generic CPL unit is modeled as shown in Fig. 5(a), where the equivalent impedance $Z_{{\rm p}j}$ ($j = 1, 2, \ldots, m$) is in the form of resistor $R_{{\rm p}j}$ and DC capacitor $C_{{\rm p}j}$ in parallel.

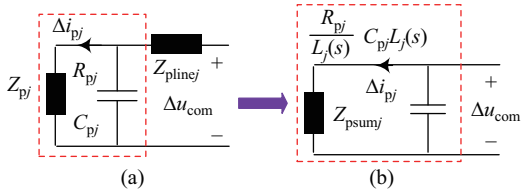

Fig. 5. Evolution of the model of the generic CPL unit. (a) The basic model. (b) The model by introducing $L_j(s)$.

Linearized at a steady operating point, the generic CPL unit has the negative resistance characteristic [28],

$$R_{{\rm p}j} = -U_{\rm com}^2/P_{{\rm CPL}j} \tag{6}$$

where $U_{\rm com}$ and $P_{{\rm CPL}j}$ are the steady-state values of the common DC bus voltage and power output of the generic CPL unit (with injecting to the generic CPL unit as positive direction).

Considering the influence of the DC line impedance $Z_{{\rm pline}j}$, the model in Fig. 5(a) is further modified shown in Fig. 5(b), and the impedance ratio $L_j(s)$ of the generic CPL unit is:

$$L_j(s) = Z_{{\rm p}j}/(Z_{{\rm p}j} + Z_{{\rm pline}j}) = Z_{{\rm p}j}/Z_{{\rm psum}j} \tag{7}$$

C. Reduced-order Modeling of MTDC System

With Figs. 4(b) and 5(b), a complete reduced-order model of the considered system in DVC timescale is obtained shown in Fig. 6. When master-slave control is adopted, $n = 1$, which means there only exists one DC voltage control unit. And when droop based peer-to-peer control is used, $n \neq 1$.

The total parallel impedance $Z_{\rm total}$ of the system can be obtained from Fig. 6 as:

$$1/Z_{\rm total} = \sum_{i=1}^{n} 1/Z_{{\rm ssum}i} + \sum_{j=1}^{m} 1/Z_{{\rm psum}j}$$

$$= \left[\sum_{i=1}^{n} K_i(s)/R_{si} + \sum_{j=1}^{m} L_j(s)/R_{pj}\right] + \frac{1}{s}\sum_{i=1}^{n} K_i(s)/L_{si} + s\left[\sum_{i=1}^{n} C_{si}K_i(s) + \sum_{j=1}^{m} C_{pj}L_j(s)\right] \quad (8)$$

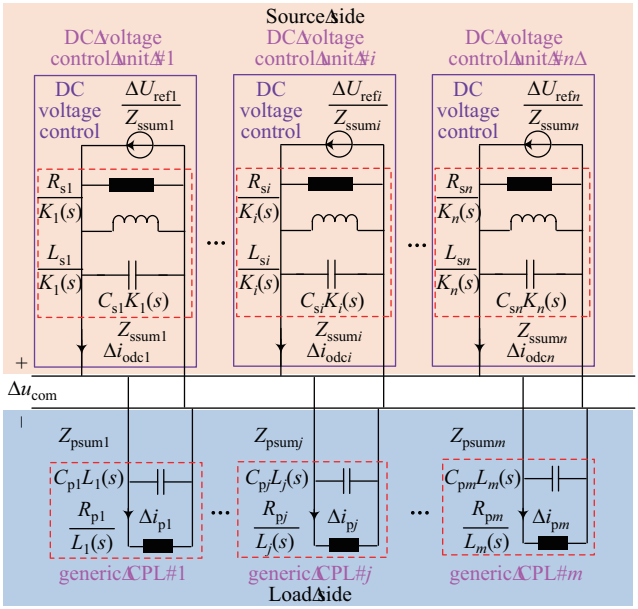

Fig. 6. Reduced-order model of the source-load MTDC system.

To analyze the system dynamic stability by observing the feature of Z_{total}, the conventional process is substituting the detailed expression of impedance ratio $K_i(s)$ in (5) and $L_j(s)$ in (7) into (8), which will make the impedance Z_{total} in a high-order form. In order to simplify the impedance Z_{total}, amplitude-frequency characteristics of $K_i(s)$ and $L_j(s)$ are first investigated shown in Fig. 7, and the detailed parameters are listed in Table I.

From Fig. 7(a), $K_i(s)$ can be simplified to a high-pass filter in low-frequency range:

$$K_i(s) = k_{\text{HPF}i}s/(s+\omega_{\text{HPF}i}) \quad (9)$$

where the corner frequency $\omega_{\text{HPF}i}$ and steady gain $k_{\text{HPF}i}$ are determined by the amplitude-frequency characteristic of $K_i(s)$.

$L_j(s)$ can be approximately regarded as 1 according to Fig. 7(b) in low-frequency range. After obtaining $\omega_{\text{HPF}i}$ and $k_{\text{HPF}i}$, substituting (9) and $L_j(s) = 1$ into (8) gives,

$$Z_{\text{total}} = 1/\left[\sum_{i=1}^{n}\frac{1}{R_{si}}\cdot\frac{k_{\text{HPF}i}s}{s+\omega_{\text{HPF}i}} + \sum_{j=1}^{m}\frac{1}{R_{pj}}\right] + \frac{1}{s}\sum_{i=1}^{n}\frac{1}{L_{si}}\cdot\frac{k_{\text{HPF}i}s}{s+\omega_{\text{HPF}i}} + s\left[\sum_{i=1}^{n} C_{si}\frac{k_{\text{HPF}i}s}{s+\omega_{\text{HPF}i}} + \sum_{j=1}^{m} C_{pj}\right] \quad (10)$$

Thus, the system dynamic stability shown in Fig. 6 will be determined by the poles of the total parallel impedance Z_{total} in (10). Since $K_i(s)$ is mimicked by a high-pass filter and $L_j(s) = 1$, the complexity of Z_{total} is reduced.

IV. Model Verification and Analysis

A. MTDC System Configuration

To verify the proposed modeling method, a low-voltage MTDC system shown in Fig. 8 has been used for theoretical analysis and PSCAD/EMTDC based simulation verification. In this system, two DC-AC converters are connected to a common DC bus through DC lines. A DC-DC converter is used to control the voltage u_{load} of load R_{load} to be a constant value to simulate a CPL unit. In master-slave control mode, DC-AC#1 adopts droop control, and DC-AC#2 adopts constant power control. In droop based peer-to-peer control mode, both

TABLE I
System Parameters of a Low-Voltage MTDC System

Terminals	Subsystem	Parameter	Value
DC-AC (DC voltage control unit)	Electrical parameters	Rated AC andDC voltages	220 V/400 V
		Rated power	400 kVA
		*LCL*filter	2 mH/10 μF, 0.5 Ω/0.12 mH
		Switching frequency	10 kHz
		DC capacitance	4000 μF
		DC line ($L_{\text{sline}}/R_{\text{sline}}$)	0.25 mH/0.48 Ω
	U_{dc}-I droop	Setting value ($u_{\text{dcref}}/i_{\text{dcset}}$)	1 pu/0 pu
		Droop gain (R_{d})/low-pass filter constant (T_{lpf})	1.25 pu/0.01 s
	DC voltage control	Proportional gain and integral gain ($k_{\text{pu}}/k_{\text{iu}}$)	0.054 pu/2.7 pu
	Current control	Proportional gain and integral gain ($k_{\text{pi}}/k_{\text{ii}}$)	9.78 pu/978 pu
DC-AC (Power control)	Electrical parameters	Rated AC andDC voltages	220 V/400 V
		*LCL*filter	2 mH/10 μF, 0.5 Ω/0.12 mH
		Switching frequency	10 kHz
		DC capacitance	4000 μF
		DC line ($L_{\text{pline}}/R_{\text{pline}}$)	0.25 mH/0.48 Ω
	Current control	Setting value (P_{set})	2 kW
		Proportional gain and integral gain ($k_{\text{pi}}/k_{\text{ii}}$)	9.78 pu/978 pu
DC-DC (CPL unit)	Electrical parameters	Rated DC load voltage	200 V
		DC load (R_{load})	12.8 Ω
		Capacitance at high voltage side	2000 μF
	Loadvoltagecontrol	$k_{\text{p}}/k_{\text{i}}$	0.1 pu/4 pu
	Current control	$k_{\text{p}}/k_{\text{i}}$	0.25 pu/250 pu

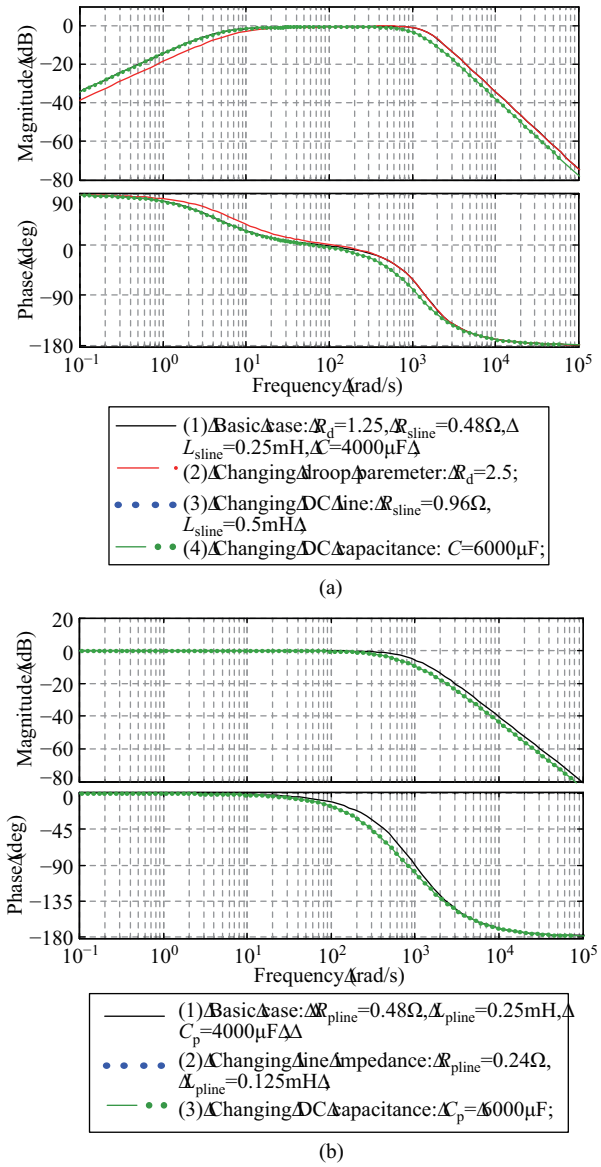

Fig. 7. Amplitude-frequency characteristics of (a) $K_i(s)$, and (b) $L_j(s)$.

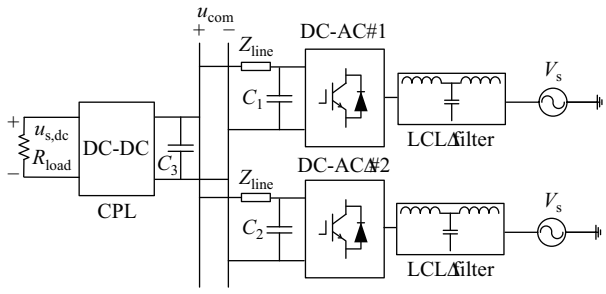

Fig. 8. Topology of thelow-voltage MTDC system.

of DC-AC#1 and DC-AC#2 adopt droop control. The main system parameters are given in Table I.

With the proposed modeling method in Section III, the corresponding reduced-order models of low-voltage MTDC systems with different system-level control strategies can be obtained as shown in Fig. 9.

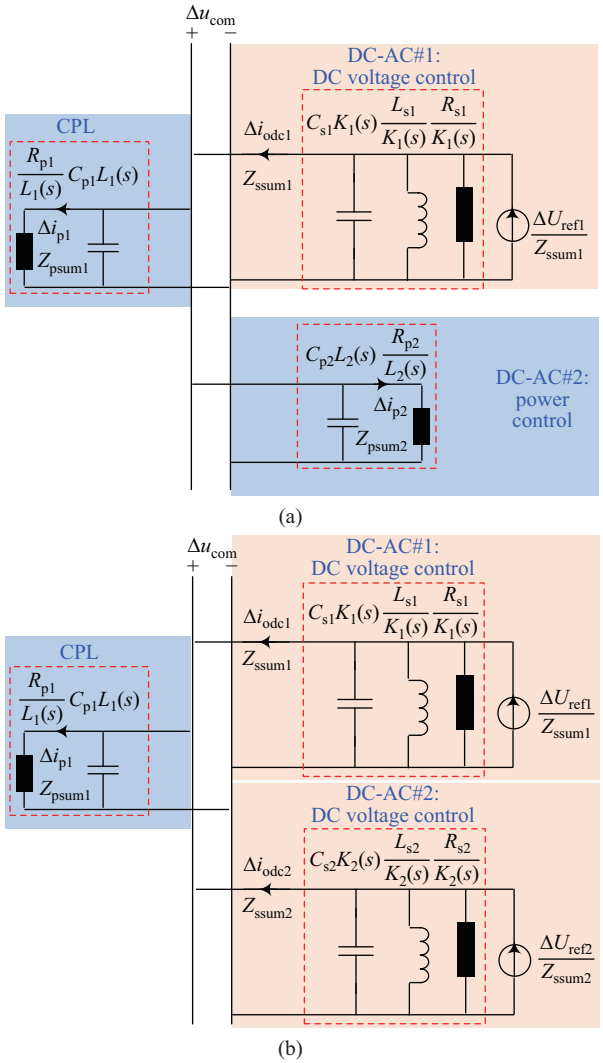

Fig. 9. Reduced-order models of the low-voltage MTDC system with different system-level control strategies. (a) The model under master-slave control mode. (b) The model under droop based peer-to-peer control mode.

B. Theoretical Analysis

1) Characteristic of $K(s)$

The characteristic of $K(s)$ is first analyzed in this subsection, as shown in Fig. 10. As can be observed, the corner frequency ω_{HPF} is primarily affected by R_{sline}, R_{d} and k_{iu}, while steady gain k_{HPF} is primarily affected by R_{sline}, R_{d} and k_{pu}. Especially, the corner frequency ω_{HPF} will be increased with the increase of R_{sline} and k_{iu}, and k_{HPF} will be increased with the decrease of k_{pu}.

With a given set of electrical and control parameters, corner frequency ω_{HPF} and steady gain k_{HPF} of $K(s)$ can be calculated first, and then the system second-order characteristic equation under master-slave control shown in Fig. 9(a) can be obtained from (10) as:

$$[C_{\mathrm{s1}}k_{\mathrm{HPF}} + (C_{\mathrm{p1}} + C_{\mathrm{p2}})]s^2 + [(1/R_{\mathrm{p1}} + 1/R_{\mathrm{p2}})\omega_{\mathrm{HPF}} + k_{\mathrm{HPF}}/L_{\mathrm{s1}}] + [k_{\mathrm{HPF}}/R_{\mathrm{s1}} + (1/R_{\mathrm{p1}} + 1/R_{\mathrm{p2}}) + (C_{\mathrm{p1}} + C_{\mathrm{p2}})\omega_{\mathrm{HPF}}]s = 0 \quad (11)$$

From (11), the system dynamic stability can be studied and designed in an analytical approach. Especially when (11) is

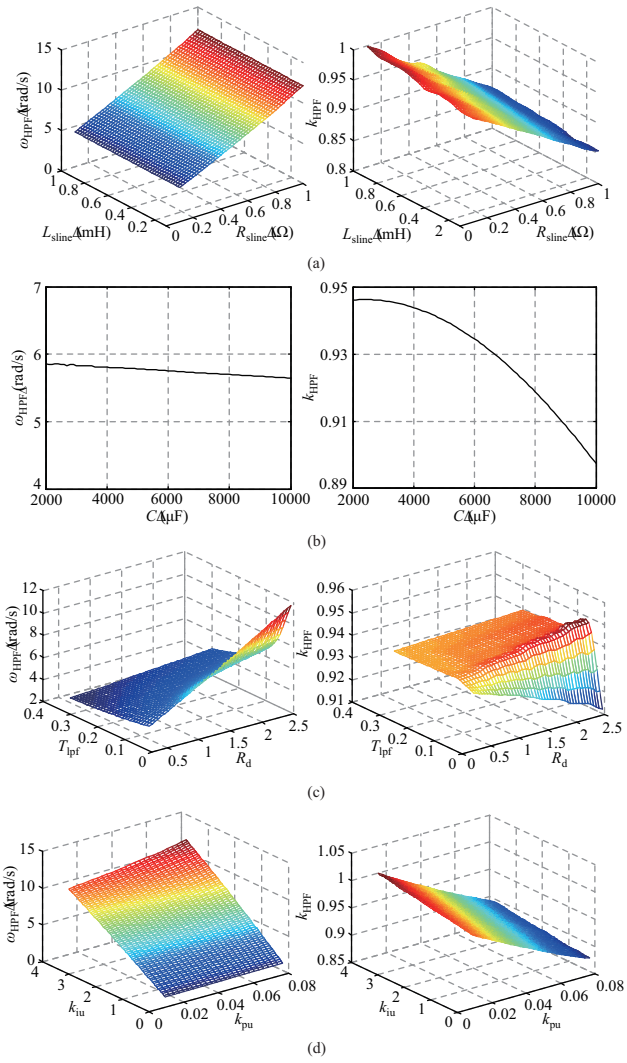

Fig. 10. ω_{HPF} and k_{HPF} corresponding to different parameters. (a) Influence of DC line.(b) Influence of DC capacitance.(c) Influence of droop control loop. (d) Influence of DC voltage control loop.

designed as a second-order under damped system ($0 < \zeta < 1$), system damping gain ζ and oscillation frequency ω_{d} under master-slave control mode can be obtained as:

$$\begin{cases} \zeta = \dfrac{1}{2} \dfrac{k_{\mathrm{HPF}}/R_{\mathrm{s1}} + (1/R_{\mathrm{p1}} + 1/R_{\mathrm{p2}}) + (C_{\mathrm{p1}} + C_{\mathrm{p2}})\omega_{\mathrm{HPF}}}{\sqrt{[C_{\mathrm{s1}}k_{\mathrm{HPF}} + (C_{\mathrm{p1}} + C_{\mathrm{p2}})][((1/R_{\mathrm{p1}} + 1/R_{\mathrm{p2}})\omega_{\mathrm{HPF}} + k_{\mathrm{HPF}}/L_{\mathrm{s1}}]}} \\ \omega_{\mathrm{d}} = \sqrt{\dfrac{(1/R_{\mathrm{p1}} + 1/R_{\mathrm{p2}})\omega_{\mathrm{HPF}} + k_{\mathrm{HPF}}/L_{\mathrm{s1}}}{C_{\mathrm{s1}}k_{\mathrm{HPF}} + (C_{\mathrm{p1}} + C_{\mathrm{p2}})}(1 - \zeta^2)} \end{cases} \tag{12}$$

2) System Oscillation Frequency and Damping

a) Influence of electrical and control parameters: Based on (12), the system dynamic stability under master-slave control can be studied by analyzing system oscillation frequency and damping in a straight forward manner, as shown in Figs. 11 and 12. As can be seen, the DC voltage control loop has significant influence on system dynamic stability in the low-frequency range, which provides the answer that why we call our research as system dynamic stability in "DVC timescale."Especially, when proportional gain k_{pu} increases,

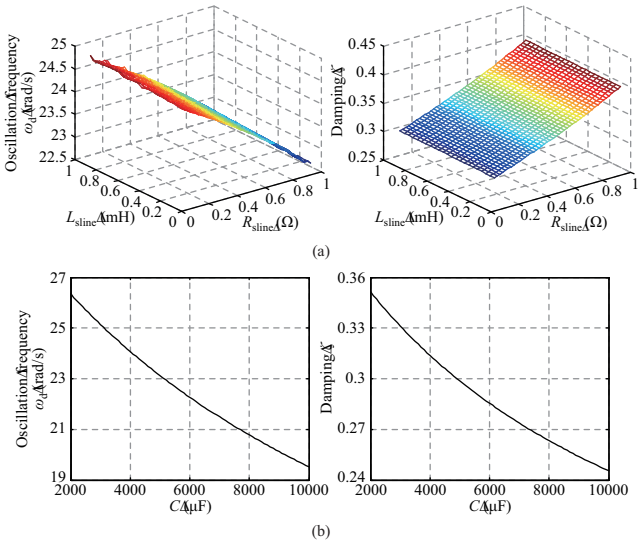

Fig. 11. Relationship between electrical parameters and oscillation frequency and damping under master-slave control mode. (a) Influence of DC line. (b) Influence of DC capacitance.

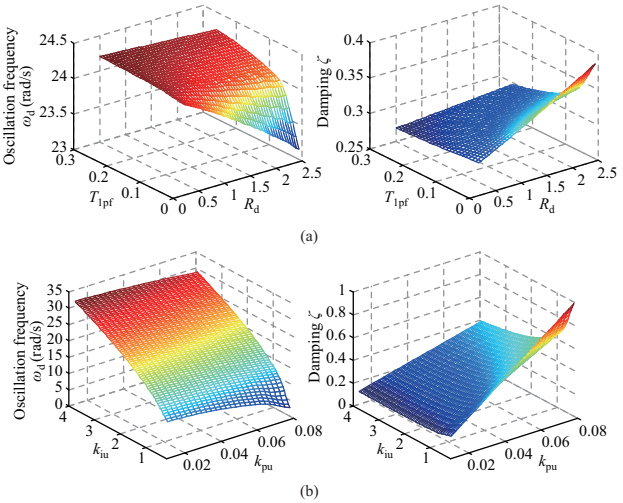

Fig. 12. Relationship between control parameters and oscillation frequency and damping under master-slave control mode. (a) Influence of droop control loop. (b) Influence of DC voltage control loop.

the system will become more damped, and a larger integral gain k_{iu} will make the oscillation frequency higher. When DC capacitance increases, the system oscillation frequency will be decreased slightly. Increasing R_{sline} will increase system damping slightly.

b) Influence of system-level control strategies: In the same way, the second-order characteristic equation of the system under droop based peer-to-peer control mode can be obtained as,

$$\begin{aligned} &[(C_{\mathrm{s1}} + C_{\mathrm{s2}})k_{\mathrm{HPF}} + C_{\mathrm{p1}}]s^2 + [\omega_{\mathrm{HPF}}/R_{\mathrm{p1}} + k_{\mathrm{HPF}}(1/L_{\mathrm{s1}} \\ &\quad + 1/L_{\mathrm{s2}})] + [k_{\mathrm{HPF}}(1/R_{\mathrm{s1}} + 1/R_{\mathrm{s2}}) + 1/R_{\mathrm{p1}} \\ &\quad + \omega_{\mathrm{HPF}}C_{\mathrm{p1}}]s = 0 \end{aligned} \tag{13}$$

From (13), system damping gain ζ and oscillation frequency ω_{d} can be further obtained as follows,

$$\begin{cases} \zeta = \dfrac{1}{2}\dfrac{k_{\mathrm{HPF}}(1/R_{\mathrm{s1}}+1/R_{\mathrm{s2}})+1/R_{\mathrm{p1}}+\omega_{\mathrm{HPF}}C_{\mathrm{p1}}}{\sqrt{[(C_{\mathrm{s1}}+C_{\mathrm{s2}})k_{\mathrm{HPF}}+C_{\mathrm{p1}}][\omega_{\mathrm{HPF}}/R_{\mathrm{p1}}+k_{\mathrm{HPF}}(1/L_{\mathrm{s1}}+1/L_{\mathrm{s2}})]}} \\ \omega_{\mathrm{d}} = \sqrt{\dfrac{\omega_{\mathrm{HPF}}/R_{\mathrm{p1}}+k_{\mathrm{HPF}}(1/L_{\mathrm{s1}}+1/L_{\mathrm{s2}})}{(C_{\mathrm{s1}}+C_{\mathrm{s2}})k_{\mathrm{HPF}}+C_{\mathrm{p1}}}(1-\zeta^2)} \end{cases} \tag{14}$$

Based on (11)–(14), system dynamic stability under different system-level control strategies can be investigated in an analytical approach shown in Fig. 13. And the relationship between the DC voltage control loop and oscillation frequency and damping under droop based peer-to-peer control is shown in Fig. 14. It can be seen that with the increase of proportional gain k_{pu}, the system root loci are both far away from the imaginary axis, and system damping are both reinforced, while the root locus under droop based peer-to-peer control changes faster and the oscillation frequency is higher. And when proportional gain k_{pu} is large, the system will be better damped under the droop based peer-to-peer control. In addition, the impact of the DC voltage control loop on system oscillation frequency and damping under droop based peer-to-peer control is similar with that under master-slave control mode.

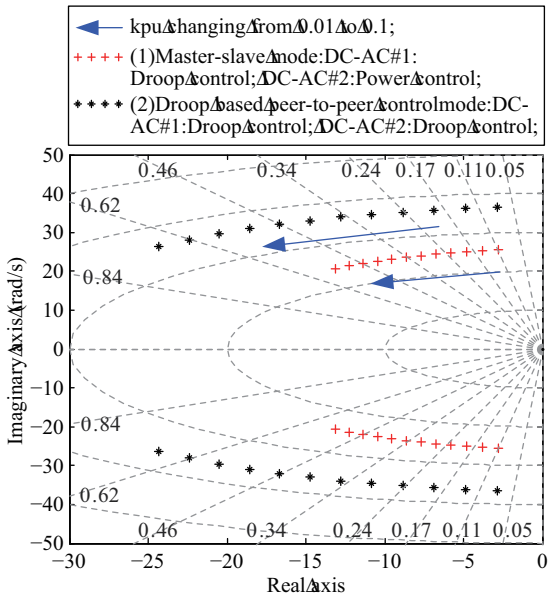

Fig. 13. System root loci under different system-level control strategies when proportional gain k_{pu} varies.

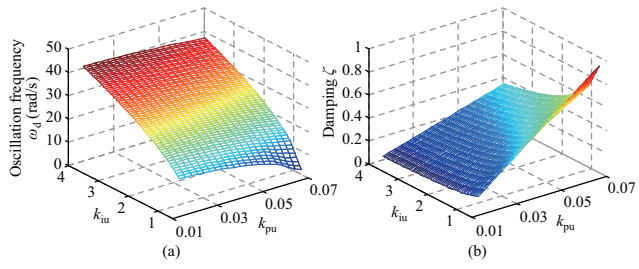

Fig. 14. The relationship between DC voltage control loop and oscillation frequency and damping under droop based peer-to-peer control mode. (a) Oscillation frequency. (b) Damping.

C. Simulation Verification

1) Simulation with Different Electrical and Control Parameters

Simulations under master-slave mode with different electrical and control parameters are conducted to verify the proposed modeling method. The load voltage u_{load} is changed from 200 V to 250 V at $t = 3$ s. Simulation results are given in Figs. 15 and 16. The theoretical calculation of damping and oscillation frequency of the reduced-order model are given in Tables II and III. It can be seen that increasing k_{pu} will increase system damping and decreasing k_{pi} will decrease oscillation frequency, and the DC line has little effect on system dynamic although it will affect the steady-state value of the common DC bus voltage. Meanwhile, the oscillation frequencies are about 22.84 rad/s of scenario 3 in Fig. 15(a) and 16.53 rad/s of scenario 7 in Fig. 16(a), which are very consistent with theoretical calculation values 22.65 rad/s in Table II and 16.48 rad/s in Table III respectively. The simulation results are in good agreement with theoretical

TABLE II
DAMPING AND OSCILLATION FREQUENCIES WITH DIFFERENT ELECTRICAL PARAMETERS

Model	Parameter	Scenario1	Scenario2	Scenario3	Scenario4
Reduced-order model	k_{HPF}	0.945	0.936	0.86	0.948
	ω_{HPF} (rad/s)	5.81	5.76	12	5.8
	ζ	0.312	0.284	0.39	0.312
	ω_{d} (rad/s)	24.16	22.26	22.65	24.19

TABLE III
DAMPING AND OSCILLATION FREQUENCIES WITH DIFFERENT CONTROL PARAMETERS

Model	Parameter	Scenario5	Scenario 6	Scenario 7	Scenario8
Reduced-order model	k_{HPF}	0.945	0.84	0.925	0.915
	ω_{HPF} (rad/s)	5.81	5.85	2.71	9.02
	ζ	0.312	0.555	0.386	0.350
	ω_{d} (rad/s)	24.16	20.38	16.48	23.53

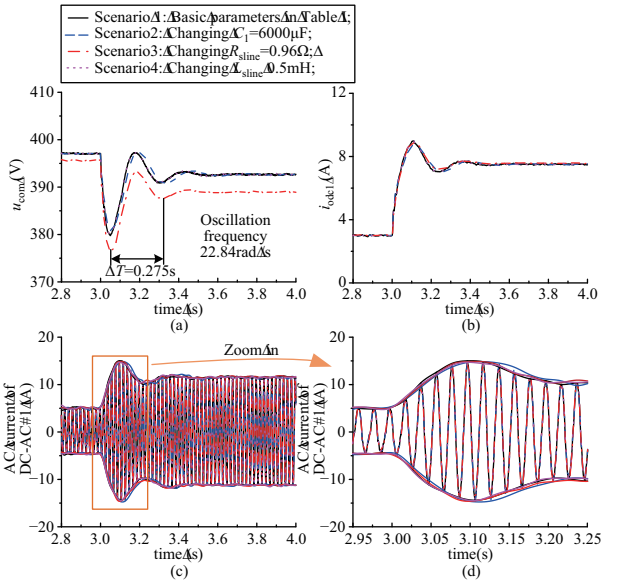

Fig. 15. Simulation results under master-slave control mode with different electrical parameters. (a) Dynamic of the common DC bus voltage. (b) Dynamics of DC current (i_{odc1}). (c) Dynamic of AC current of DC-AC#1. (d) Partial enlarged view of AC current of DC-AC#1.

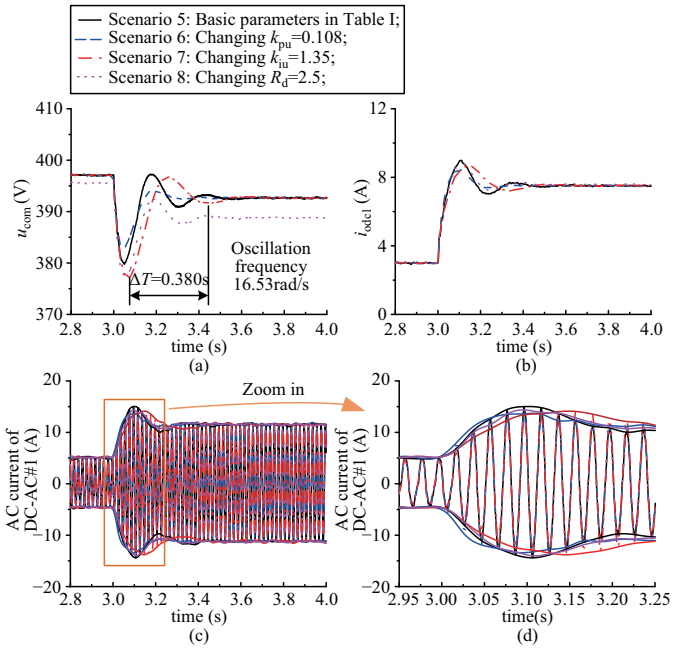

Fig. 16. Simulation results under master-slave control mode with different control parameters. (a) Dynamics of the common DC bus voltage. (b) Dynamics of DC current (i_{odc1}). (c) Dynamic of AC current of DC-AC#1. (d) Partial enlarged view of AC current of DC-AC#1.

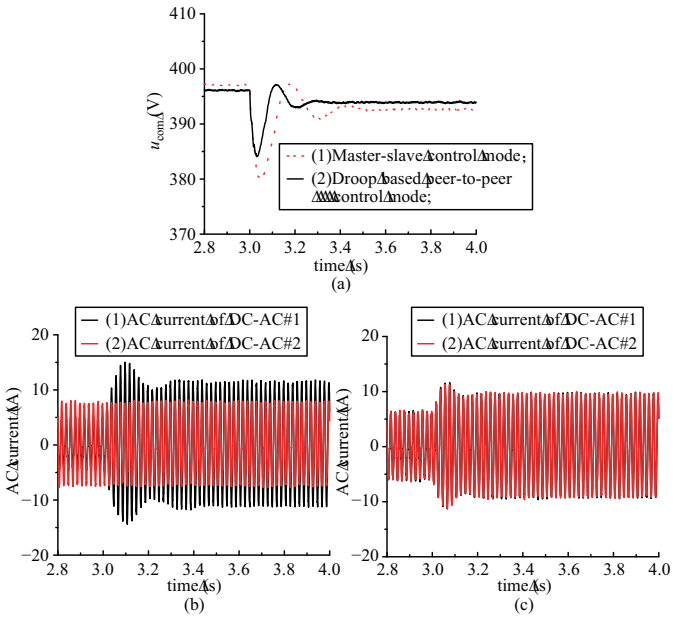

Fig. 17. Simulation results with different system-level control strategies when $k_{\rm pu}$ = 0.054. (a) Common DC bus voltage ($u_{\rm com}$). (b) AC current under master-slave control mode. (c) AC current under droop based peer-to-peer control model.

analysis, the effectiveness of the proposed modeling method is verified.

2) Simulation with Different System-level Control Strategies

With the same transient mentioned above, two conditions under different system-level control strategies are studied as shown in Fig. 17. As can be observed, the voltage dynamic of the common DC bus is better damped and oscillation frequency is higher under the droop based peer-to-peer control, which is in good agreement with theoretical analysis. Meanwhile, under master-slave control, only DC-AC#1 responds to the load changing, which leads to a bigger AC current of DC-AC#1 compared with that under the droop based peer-to-peer control.

V. Experimental Verification

To verify the proposed modeling method, the experimental system shown in Fig. 8 has been built. The control and corresponding parameters of the experimental system are the same with the simulation system mentioned above. At time t, the load voltage $u_{\rm load}$ is changed from 200V to 250V, the experimental result under master-slave control mode is given in Fig. 18. The oscillation frequency after transient is 24.17 rad/s, which is consistent with the calculated value 24.16 rad/s in Table II, the effectiveness of the proposed modeling method is validated.

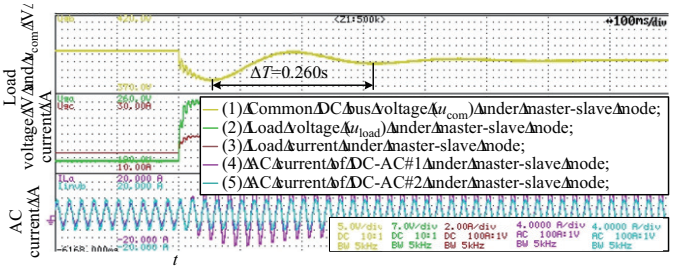

Fig. 18. Experiment result under master-slave control mode.

A. Experiment with Different System Electrical and Control Parameters

At time t = 0.2 s, the load voltage $u_{\rm load}$ is changed from 200 V to 250 V. The experimental results under master-slave mode with different electrical and control parameters are shown in Fig. 19. It can be seen that the damping will be increased with the increase of the proportional gain of the DC voltage control, with a smaller integral gain, the oscillation frequency will be lower. And changing the DC line resistance and droop gain have little effect on system dynamic although they will affect the stead-state value of the common DC bus voltage. Meanwhile, the oscillation frequencies are about 22.77 rad/s of scenario 3 in Fig. 19(a) and 16.45 rad/s of scenario 6 in Fig. 19(b), which are very consistent with the simulation results 22.84 rad/s of scenario 3 in Fig. 15(a) and 16.53 rad/s of scenario 7 in Fig. 16(a) respectively.

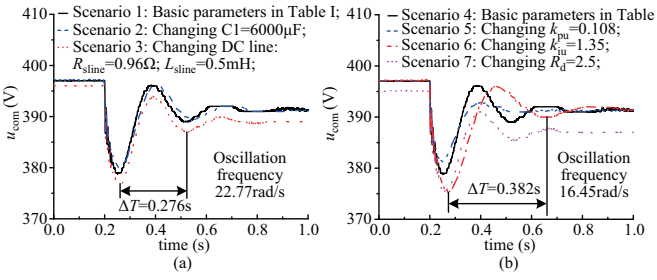

Fig. 19. Experiment results under master-slave control mode with different electrical and control parameters. (a) Results with different electrical parameters. (b) Results with different control parameters.

B. Experiment with Different System-level Control Strategies

At time t, the load voltage u_{load} is changed from 200 V to 250 V. The experimental results under different system-level control strategies are shown in Fig. 20. It can be seen that under droop based peer-to-peer control mode, the voltage dynamic of the common DC bus is better damped and the oscillation frequency is higher compared with that under master-slave control mode. Meanwhile, both of DC-AC#1 and DC-AC#2 can respond to the load changing under droop based peer-to-peer control mode, and their AC current dynamics and steady-state values are almost the same since they have the same control parameters. The experimental results are in good agreement with the simulation results.

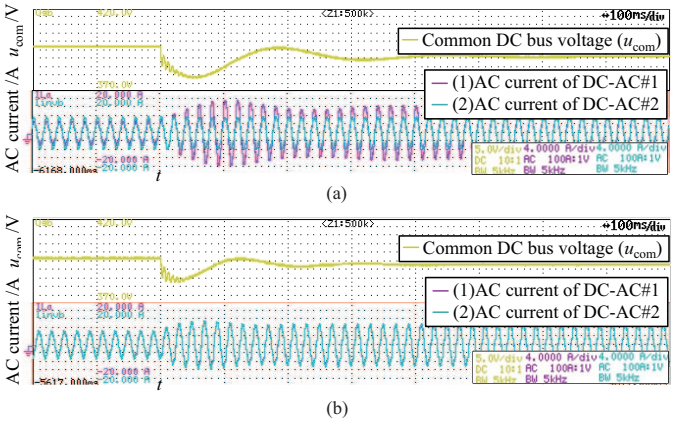

Fig. 20. Experiment results with different system-level control strategies when $k_{\text{pu}} = 0.054$. (a) Master-slave control mode. (b) Droop based peer-to-peer control mode.

VI. Conclusion

This paper proposes a reduced-order model in the form of parallel *RLC* structure for dynamic stability of the MTDC system in DVC timescale. And the physical meaning of control parameters is revealed in an intuitive way. With this model, the second-order characteristic equation is obtained, which makes it easy to investigate system dynamic stability in an analytical approach. The influence of electrical and control parameters on system oscillation frequency and damping have been characterized in a straight forward manner. It can also be found that the DC voltage control loop plays an important role in system dynamic stability, which answers the reason why it is called "DC voltage control timescale." In addition, dynamic stability of the considered system with different system-level control strategies has been well investigated.

This paper only focuses on dynamic stability of MTDC systems, how to take the influence of interconnected AC systems into consideration, and further analyze dynamic stability of the complete hybrid AC/DC system will be our future study.

References

[1] F. H. Guo, L. Wang, C. Y. Wen, D. Zhang, and Q. W. Xu, "Distributed voltage restoration and current sharing control in islanded DC microgrid systems without continuous communication," *IEEE Transactions on Industrial Electronics*, vol. 67, no. 4, pp. 3043–3053, Apr. 2020.

[2] W. Pei, W. Deng, X. Zhang, H. Qu, and K. Sheng, "Potential of using multiterminal LVDC to improve plug-in electric vehicle integration in an existing distribution network," *IEEE Transactions on Industrial Electronics*, vol. 62, no. 5, pp. 3101–3111, May 2015.

[3] R. Wang, L. J. Chen, T. W. Zheng, and S. W. Mei, "VSG-based adaptive droop control for frequency and active power regulation in the MTDC system," *CSEE Journal of Power and Energy Systems*, vol. 3, no. 3, pp. 260–268, Sep. 2017.

[4] X. L. Li, L. Guo, C. Hong, Y. Zhang, Y. W. Li, and C. S. Wang, "Hierarchical control of multiterminal DC grids for large-scale renewable energy integration," *IEEE Transactions on Sustainable Energy*, vol. 9, no. 3, pp. 1448–1457, Jul. 2018.

[5] J. LagoandM. L. Heldwein, "Operation and control-oriented modeling of a power converter for current balancing and stability improvement of DC active distribution networks," *IEEE Transactions on Power Electronics*, vol. 26, no. 3, pp. 877–885, Mar. 2011.

[6] L. Guo, Y. B. Feng, X. L. Li, C. S. Wang, and Y. W. Li, "Stability analysis of a DC microgrid with master-slave control structure," in *2014 IEEE Energy Conversion Congress and Exposition*, 2014, pp. 5682–5689.

[7] J. Lai, X. Q. Lu, X. H. Yu, W. Yao, J. Y. Wen, and S. J. Cheng, "Distributed multi-DER cooperative control for master-slave-organized microgrid networks with limited communication bandwidth," *IEEE Transactions on Industrial Informatics*, vol. 15, no. 6, pp. 3443–3456, Jun. 2019.

[8] A. Kirakosyan, E. F. El-Saadany, M. S. E. Moursi, and K. A. Hosani, "DC voltage regulation and frequency support in pilot voltage droop-controlled multiterminal HVDC systems," *IEEE Transactions on Power Delivery*, vol. 33, no. 3, pp. 1153–1164, Jun. 2018.

[9] W. Wang, M. Barnes, and O., Marjanovic, "Stability limitation and analytical evaluation of voltage droop controllers for VSC MTDC," *CSEE Journal of Power and Energy Systems*, vol. 4, no. 2, pp. 238–249, Jun. 2018.

[10] X. Zhang, X. B. Ruan, and C. K. Tse, "Impedance-based local stability criterion for DC distributed power systems," *IEEE Transactions on Circuits and Systems I: Regular Papers*, vol. 62, no. 3, pp. 916–925, Mar. 2015.

[11] A. Riccobono and E. Santi, "Comprehensive review of stability criteria for DC power distribution systems," *IEEE Transactions on Industry Applications*, vol. 50, no. 5, pp. 3525–3535, Sep. /Oct. 2014.

[12] D. Marx, P. Magne, B. Nahid-Mobarakeh, S. Pierfederici, and B. Davat, "Large signal stability analysis tools in DC power systems with constant power loads and variable power loads—a review," *IEEE Transactions on Power Electronics*, vol. 27, no. 4, pp. 1773–1787, Apr. 2012.

[13] H. Yuan, X. M. Yuan, and J. B. Hu, "Modeling of grid-connected VSCs for power system small-signal stability analysis in DC-link voltage control timescale," *IEEE Transactions on Power Systems*, vol. 32, no. 5, pp. 3981–3991, Sep. 2017.

[14] Y. H. Huang, X. B. Zhai, J. B. Hu, D. Liu, and C. Lin, "Modeling and stability analysis of VSC internal voltage in DC-link voltage control timescale," *IEEE Journal of Emerging and Selected Topics in Power Electronics*, vol. 6, no. 1, pp. 16–28, Mar. 2018.

[15] Y. H. Huang, X. M. Yuan, J. B. Hu, P. Zhou, and D. Wang, "DC-bus voltage control stability affected by AC-bus voltage control in VSCs connected to weak AC grids," *IEEE Journal of Emerging and Selected Topics in Power Electronics*, vol. 4, no. 2, pp. 445–458, Jun. 2016.

[16] Y. H. Huang, X. M. Yuan, J. B. Hu, and P. Zhou, "Modeling of VSC connected to weak grid for stability analysis of DC-link voltage control," *IEEE Journal of Emerging and Selected Topics in Power Electronics*, vol. 3, no. 4, pp. 1193–1204, Dec. 2015.

[17] Y. H. Huang, D. Wang, L. Shang, G. R. Zhu, H. Y. Tang, and Y. Li, "Modeling and stability analysis of DC-link voltage control in multi-VSCs with integrated to weak grid," *IEEE Transactions on Energy Conversion*, vol. 32, no. 3, pp. 1127–1138, Sep. 2017.

[18] T. Dragičević, X. N. Lu, J. C. Vasquez, and J. M. Guerrero, "DC microgrids-Part I: A review of control strategies and stabilization techniques," *IEEE Transactions on Power Electronics*, vol. 31, no. 7, pp. 4876–4891, Jul. 2016.

[19] N. Rashidirad, M. Hamzeh, K. Sheshyekani, and E. Afjei, "A simplified equivalent model for the analysis of low-frequency stability of multi-bus DC microgrids," *IEEE Transactions on Smart Grid*, vol. 9, no. 6, pp. 6170–6182, Nov. 2018.

[20] N. Rashidirad, M. Hamzeh, K. Sheshyekani, and E. Afjei, "High-frequency oscillations and their leading causes in DC microgrids," *IEEE Transactions on Energy Conversion*, vol. 32, no. 4, pp. 1479–1491, Dec. 2017.

[21] M. F. Wu and D. D. C. Lu, "A novel stabilization method of LC input filter with constant power loads without load performance compromise

in DC microgrids," *IEEE Transactions on Industrial Electronics*, vol. 62, no. 7, pp. 4552–4562, Jul. 2015.
[22] X. L. Li, L. Guo, S. H. Zhang, C. S. Wang, Y. W. Li, A. W. Chen, and Y. B. Feng, "Observer-based DC voltage droop and current feed-forward control of a DC microgrid," *IEEE Transactions on Smart Grid*, vol. 9, no. 5, pp. 5207–5216, Sep. 2018.
[23] S. Anand and B. G. Fernandes, "Reduced-order model and stability analysis of low-voltage DC microgrid," *IEEE Transactions on Industrial Electronics*, vol. 60, no. 11, pp. 5040–5049, Nov. 2013.
[24] X. L. Li, L. Guo, Y. W. Li, C. Hong, Y. Zhang, Z. Guo, D. Huang, and C. S. Wang, "Flexible interlinking and coordinated power control of multiple DC microgrids clusters," *IEEE Transactions on Sustainable Energy*, vol. 9, no. 2, pp. 904–915, Apr. 2018.
[25] L. Guo, P. F. Li, X. L. Li, D. Huang, and J. B. Zhu, "Flexible control of DC interlinked multiple MGs cluster," *IET Generation Transmission & Distribution*, vol. 13, no. 11, pp. 2088–2101, Jun. 2019.
[26] Y. F. Li, G. F. Tang, J. Ge, Z. Y. He, H. Pang, J. Yang, and Y. N. Wu, "Modeling and damping control of modular multilevel converter based DC grid," *IEEE Transactions on Power Systems*, vol. 33, no. 1, pp. 723–735, Jan. 2018.
[27] F. Gao, S. Bozhko, A. Costabeber, C. Patel, P. Wheeler, C. I. Hill, and G. Asher, "Comparative stability analysis of droop control approaches in voltage-source-converter-based DC microgrids," *IEEE Transactions on Power Electronics*, vol. 32, no. 3, pp. 2395–2415, Mar. 2017.
[28] S. Singh, A. R. Gautam, and D. Fulwani, "Constant power loads and their effects in DC distributed power systems: A review," *Renewable and Sustainable Energy Reviews*, vol. 72, pp. 407–421, May 2017.

Li Guo (M'11) received his B.Sc. and Ph.D. degree in Electrical Engineering from South China University of Technology in 2002 and 2007, respectively.

Dr. Guo is currently a full Professor at Tianjin University. His research interests include the optimal planning and design of microgrid, the coordinated operating strategy of microgrid, and the advanced energy management system.

Pengfei Li received his B.Sc. degree from Taiyuan University of Technology, Shanxi, China, in 2014, and the M. Sc. degree from Zhejiang University, Hangzhou, China, in 2017, both in Electrical Engineering.

He is currently working toward the Ph.D. degree in Electrical Engineering at Tianjin University, Tianjin, China. His current research interests include modeling, stability analysis and control of power electronics dominated power systems.

Xialin Li (M'15) received his B.Sc. degree and the Ph.D. degree from Tianjin University, Tianjin, China, in 2009 and 2014, respectively.

Since 2014, he has been a lecture with the School of Electrical Engineering and Automation, Tianjin University, China. In 2016, under the State Scholarship Fund, he was invited as a Visiting Professor to the Department of Electrical and Computer Engineering, University of Alberta, Canada. His current research interests include the modeling and control of power converters, distributed generation, hybrid ac/dc microgrid, and multi-terminal dc grids (MTDC).

Fei Gao received his Ph.D. degree in Electrical Engineering from the Power Electronics, Machines, and Control (PEMC) Research Group, University of Nottingham, Nottingham, UK, in 2016. From Mar. 2010 to Sep. 2012, he has worked in Jiangsu Electric Power Research Institute, Nanjing, State Grid Corporation of China. From 2016 to 2019, he has been with Department of Engineering Science, University of Oxford, UK as a postdoctoral researcher. Since July 2019 he joined Shanghai Jiao Tong University as an Associate Professor. His current research interests include modeling, control, power management and stability of microgrids and more electric transportation systems. Dr. Gao won the European Union Clean Sky Best Ph.D. Award in 2017 and IET Control & Automation Runner Up Ph.D. Award in 2018.

Di Huang received his B.S. and M.S. degrees in Electric Engineering from Tianjin University in 2017 and 2020, respectively.

He is currently with Guangzhou Power Supply Bureau of Guangdong Power Grid Co., Ltd.. His research interests in the flexible DC transmission and distribution system.

Chengshan Wang (SM'11) received the B.Sc. degree, the M.Sc. Degree and the Ph.D. degree from Tianjin University, Tianjin, China, in 1983, 1985 and 1991, respectively.

He became a Full Professor of Tianjin University in 1996. He has been to Cornell University as a visiting scientist from 1994 to 1996 and to Carneigie Mellon University as a visiting professor from 2001 to 2002. Prof. Wang is the gainer of Fok Ying Tung Fund, Excellent Young Teacher Fund of Education Ministry and a winner of National Science Fund for Distinguished Young Scholars. He is the Chief Scientist of 973 project, "Research on the Key Issues of Distributed Generation Systems" from 2009 to 2013 that was participated by Chinese power engineering scientists from 8 leading institutions. His research is in the area of distribution system analysis and planning, distributed generation system and microgrid, and power system security analysis.